Supplementary Information

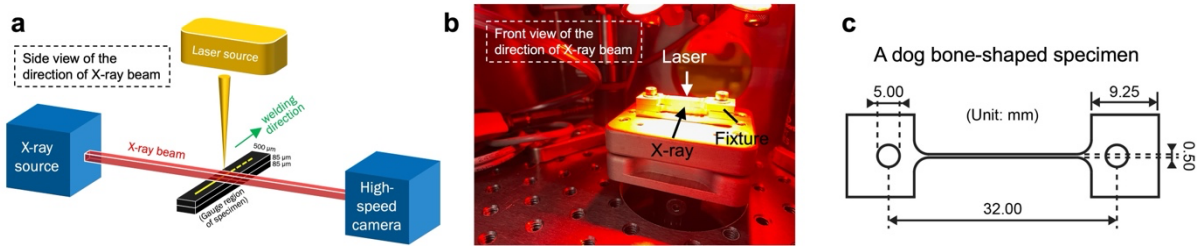

Supplementary Fig. 1: Experimental setup of in situ high-speed synchrotron X-ray imaging at ANL

a The side and **b** the front views of the direction of X-ray beam. The laser welding configuration was an overlapped weld. **c** Geometry of the dog bone-shaped specimen. Narrow width (500 μm) in the gauge region is required due to the strong attenuation of X-ray on stainless steel.

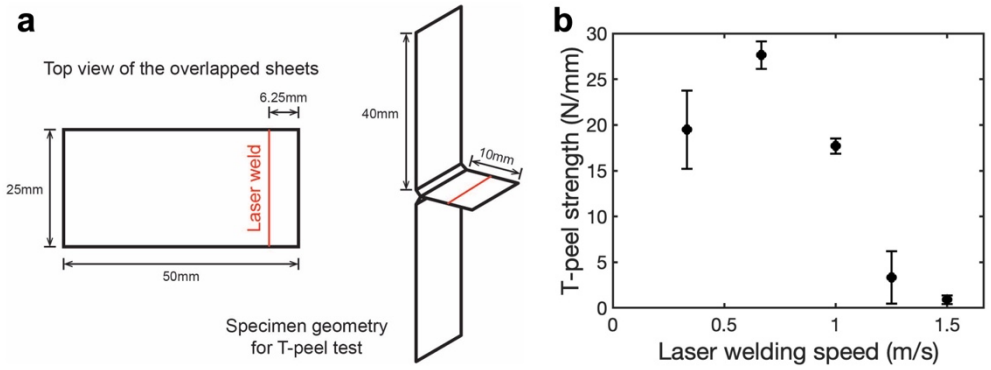

Supplementary Fig. 2: T-peel strengths of laser welds

a The configuration of laser welds made in EWI and the specimen geometry for T-peel test, which followed refs. [1,2]. **b** T-peel strengths of laser welds (defined as the load per unit length of weld). The error bars represent the standard deviation calculated from 3 measurements for each condition.

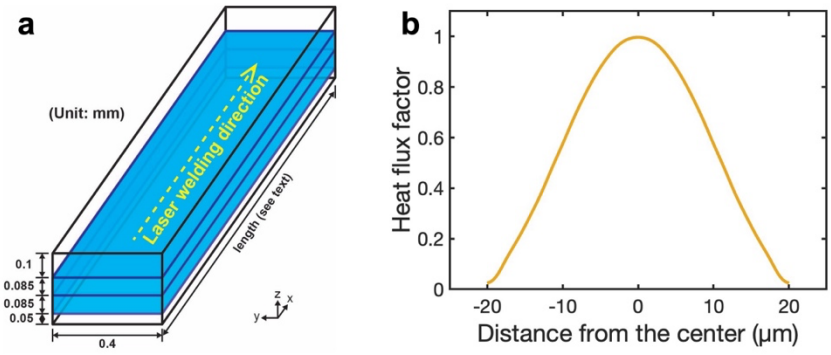

Supplementary Fig. 3 CFD simulation setup

a Dimensions of the CFD simulation domain. **b** Heat flux factor which describes the laser profile with a Gaussian distribution.

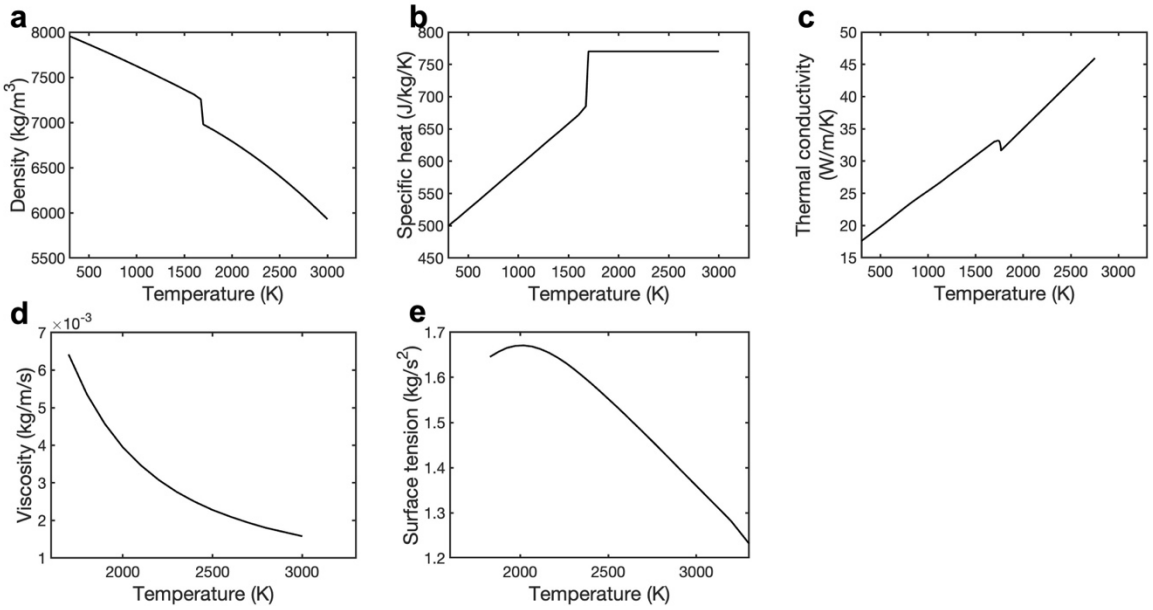

Supplementary Fig. 4 Thermophysical properties of stainless steel

a Density, **b** specific heat, **c** thermal conductivity, **d** viscosity, and **e** surface tension. They were obtained from references [3–5].

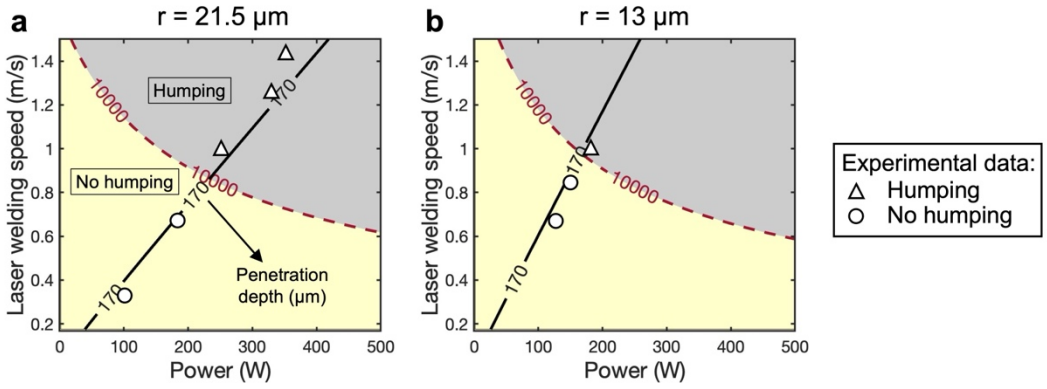

Supplementary Fig. 5 Experimental validation of onset threshold of humping predicted by dimensionless humping index (π_h)

Experimental results along with the onset threshold of humping (π_h of 10,000) and the isoline of penetration depth of 170 μm for spot radii (r) of **a** 21.5 μm and **b** 13 μm.

Supplementary Table 1: Laser process parameters

All laser process parameters with the corresponding heat inputs calculated by the equation (Heat input $= P \times \eta / u_w$ [6]). η (overall welding efficiency) is taken as 0.80 from the ref. [7].

Laser welding speed (u_w) (m/s)	Power (P) (W)	Heat input (J/m)
0.33	102	247.27
0.67	188	224.48
1.00*	249	199.20
1.25*	323	206.72
1.42*	348	196.06

*Humping occurred

Supplementary Table 2 Materials constants used in Equation 1–3 and 5 (obtained from ref. [3–5])

Material's constants	Values at T_m	Values at T_b
Density (ρ)	$7000\,\frac{kg}{m^3}$	$6000\,\frac{kg}{m^3}$
Thermal conductivity (k)	$30\,\frac{W}{m \cdot K}$	$45\,\frac{W}{m \cdot K}$
Specific heat (c_p)	$770\,\frac{J}{kg \cdot K}$	$770\,\frac{J}{kg \cdot K}$
Surface tension coefficient (γ)	$1.65\,\frac{kg}{s^2}$	$1.30\,\frac{kg}{s^2}$
Boiling temperature (T_b)	$3134\ K$	
Melting temperature (T_m)	$1698\ K$	
Ambient temperature (T_0)	$300\ K$	
Latent heat of fusion (L_m)	$2.6\times10^5\,\frac{J}{kg}$	

Supplementary Table 3 Validation of CFD simulation models, including molten pool (MP) dimensions (length, width, depth) and humping characteristics (linear number density and average height of humps)

Condition	Feature	Experiment	CFD simulation	Error (%)
0.33 m/s, 102 W	MP length (μm)	368*	400	8.7
	MP width (μm)	116^	120	3.4
	MP depth (μm)	170*	170	0
1.42 m/s, 348 W	MP length (μm)	1080*	1180	9.3
	MP width (μm)	93^	100	7.5
	MP depth (μm)	170*	170	0
	Linear number density of humps (#/mm)	1.50^	1.46	2.7
	Average height of humps (μm)	58.70 ± 14.82^	53.00 ± 15.36	9.7

* From in situ synchrotron X-ray imaging of laser welding process

^ From optical profilometry of the top surfaces of laser welds

Supplementary Table 4 The maximum melt velocity (u_{max}) from analytical calculations using Equation 1 (Beck et al. [8]) and CFD simulations

Condition	Feature	Analytical calculation	CFD simulation	Error (%)
0.33 m/s, 102 W	Maximum melt velocity (u_{max}, m/s)	0.86	0.92	7.0
1.42 m/s, 348 W		6.05	5.69	6.0

Supplementary References

1. Das, A., Fritz, R., Finuf, M. & Masters, I. Blue laser welding of multi-layered AISI 316L stainless steel micro-foils. *Opt Laser Technol* 132, 106498 (2020).

2. Standard Test Method for Peel Resistance of Adhesives (T-Peel Test). *ASTM D1876*.

3. Chen, N. *et al.* Microstructural characteristics and crack formation in additively manufactured bimetal material of 316L stainless steel and Inconel 625. *Addit Manuf* 32, 101037 (2020).

4. Kim, C. S. Thermophysical properties of stainless steels. *Argonne National Lab., Ill. (USA)* (1975).

5. Meng, X., Qin, G. & Zou, Z. Investigation of humping defect in high speed gas tungsten arc welding by numerical modelling. *Mater Des* 94, 69–78 (2016).

6. Benyounis, K. Y., Olabi, A. G. & Hashmi, M. S. J. Effect of laser welding parameters on the heat input and weld-bead profile. *J Mater Process Technol* 164–165, 978–985 (2005).

7. Fuerschbach, P. W. Measurement and prediction of energy transfer efficiency in laser beam welding. 75, (1996).

8. Beck, M., Berger, P., Dausinger, F. & Huegel, H. Aspects of keyhole/melt interaction in high-speed laser welding. in *Proc.SPIE* vol. 1397 769–774 (1991).